Nat Hazards (2015) 78:681–697
DOI 10.1007/s11069-015-1740-8

ORIGINAL PAPER

Landslide susceptibility modeling assisted by Persistent Scatterers Interferometry (PSI): an example from the northwestern coast of Malta

Daniela Piacentini[1] · Stefano Devoto[2] · Matteo Mantovani[3] · Alessandro Pasuto[3] · Mariacristina Prampolini[4] · Mauro Soldati[4]

Received: 10 September 2014 / Accepted: 6 April 2015 / Published online: 21 May 2015
© Springer Science+Business Media Dordrecht 2015

Abstract Persistent Scatterers Interferometry (PSI) techniques are widely employed in geosciences to detect and monitor landslides with high accuracy over large areas, but they also suffer from physical and technological constraints that restrict their field of application. These limitations prevent us from collecting information from several critical areas within the investigated region. In this paper, we present a novel approach that exploits the results of PSI analysis for the implementation of a statistical model for landslide susceptibility. The attempt is to identify active mass movements by means of PSI and to avoid, as input data, time-/cost-consuming and seldom updated landslide inventories. The study has been performed along the northwestern coast of Malta (central Mediterranean Sea), where the peculiar geological and geomorphological settings favor the occurrence of a series of extensive slow-moving landslides. Most of these consist in rock spreads, evolving into block slides, with large limestone blocks characterized by scarce vegetation and proper inclination, which represent suitable natural radar reflectors for applying PSI. Based on geomorphometric analyses and geomorphological investigations, a series of landslide predisposing factors were selected and a susceptibility map created. The result was validated by means of cross-validation technique, field surveys and global navigation satellite system in situ monitoring activities. The final outcome shows a good reliability and could represent an adequate response to the increasing demand for effective and low-cost tools for landslide susceptibility assessment.

✉ Matteo Mantovani
matteo.mantovani@irpi.cnr.it

[1] Department of Earth, Life and Environment Sciences, University of Urbino, Campus "E. Mattei", 61029 Urbino, Italy

[2] Department of Mathematics and Geosciences, University of Trieste, Via Weiss 2, 34127 Trieste, Italy

[3] National Research Council of Italy, Research Institute for Geo-Hydrological Protection (CNR-IRPI), Padua, Corso Stati Uniti 4, 35127 Padua, Italy

[4] Department of Chemical and Geological Sciences, University of Modena and Reggio Emilia, Largo S. Eufemia 19, 41121 Modena, Italy

Keywords Landslides · PSI · WoE · Susceptibility · Malta · Mediterranean Sea

1 Introduction

In the last years, the demand for new reliable and cost-effective methods to face natural events, such as landslides, to improve land-use planning and to reduce risks for the population has considerably increased. This is especially true for coastal areas affected by rapid and heavy urbanization and significant growth in population (Soldati et al. 2011; Martino and Mazzanti 2014). In both land surveillance and emergency management, monitoring activities are essential, since they contribute to decrease the vulnerability of the elements at risk. The major role recently played by monitoring systems is strictly connected to the development of innovative and reliable technologies. Among these, the Persistent Scatterers Interferometry (PSI) technique certainly represents one of the most recognized methods to measure, with unprecedented accuracy, landslide displacements at a regional scale (Ferretti et al. 2001; Werner et al. 2003; Costantini et al. 2008). Nevertheless, just like any remotely sensed technique, even PSI analysis cannot cope with some technical limitations that prevent from collecting measurements in several areas within the image frame (Raucoules et al. 2007). In these cases, in situ traditional monitoring methods can be applied. Clearly, it is not possible to monitor all the landslides within a region, yet we can assess where landslides are likely to occur implementing susceptibility models.

As reported by Cascini (2008), the lack of standard procedures is one of the reasons that lead to the use of different methods for the production of landslide susceptibility maps: (1) landslide inventories, (2) heuristic methods, (3) statistical analysis and (4) deterministic approaches (Guzzetti et al. 1999; Castellanos Abella and van Westen 2008; van Westen et al. 2008; Piacentini et al. 2012).

Statistical analysis methods allow defining the spatial probabilities of occurrences of a "supporting evidence," considering the distribution of causal factors. They are funded on the assumption that future landslides will occur under similar conditions to those contributing to previously occurred landslides and that predisposing factors remain constant over time (Guzzetti et al. 1999; Cardinali et al. 2002; Lan et al. 2004; Regmi et al. 2010; Piacentini et al. 2012; Galve et al. 2015).

Generally, the "supporting evidence" is the landslides themselves, mapped in *ad hoc* inventories. Unfortunately, detailed landslide inventories are time- and cost-consuming; hence, they are seldom complete and up-to-date. Consequently, it is quite rare to find available and reliable data to perform this type of analysis. In the attempt to overcome this limitation, we have tested the possibility to exploit PSI technique results, accessible and accurate at a regional scale, as "supporting evidence" to train and validate a landslide susceptibility model. The use of PSI data for this scope is yet constrained (Oliveira et al. 2014) being the direct use of PSI generally limited to update landslide inventories and assess the related hazard (Cigna et al. 2013; Lu et al. 2014; Righini et al. 2012).

We applied this novel approach to the northwestern coast of Malta (central Mediterranean Sea) that is affected by tens of extensive slow-moving landslides.

The predisposing factors for the statistical analysis were chosen based on geomorphological observations reported on published articles (Magri et al. 2008; Devoto et al. 2012) and on a LiDAR-derived DTM. The reliability of the model results was verified through a cross-validation approach, field surveys and global navigation satellite system (GNSS) measurement campaigns.

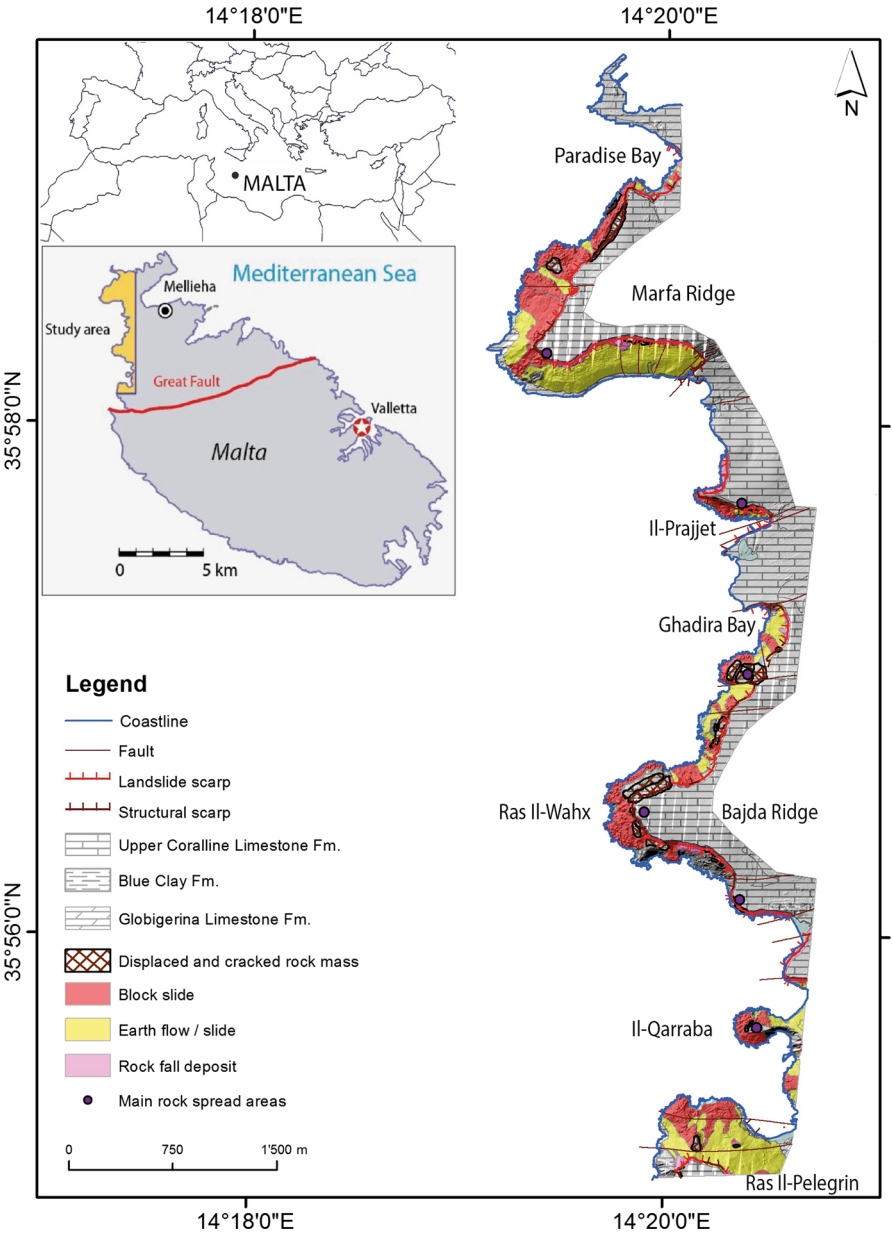

Fig. 1 Location and simplified geological–geomorphological sketch of the study area (modified from Devoto et al. 2012)

2 Study area

Malta is the main island of the Maltese archipelago placed in the central Mediterranean Sea (Fig. 1). The study area comprises the NW coast of Malta and is limited northerly by Paradise Bay and southerly by an E–W-oriented tectonic discontinuity, named Great Fault,

which crosses the island and structurally divides it into two sectors (Jongsma et al. 1985; Dart et al. 1993; Civile et al. 2010). The study area is characterized by a horst and graben system that generates an alternation of lowlands and plateaus (Illies 1981): the graben corresponding to valleys and the horst to wide karst plateaus. The latter are made up of Upper Coralline Limestone Formation (Pedley and Clarke 2002) and limited by cliffs, which overlie Blue Clay gentle slopes (Alexander 1988; Devoto et al. 2012). Clayey terrains, partially used for agricultural activities (Cyffka and Bock 2008), are abundant along the coastline and make up wide portions of Ras Il-Pelegrin promontory, Il-Qarraba peninsula, Bajda Ridge, Il-Prajjet and western side of Marfa Ridge.

The alternation of resistant limestone over "plastic" clays (Dykes 2002; Pasuto and Soldati 2013) in addition to the combination of structural and karst processes causes the occurrence of slow-moving landslides (Fig. 2). Most of these gravitational processes consist in rock spreads, which often evolve into block slides (Devoto et al. 2013).

The numerous fractures, fissures and joints favored by the different mechanical properties of limestone and clays enable rainfall infiltration and rock spreading. The presence of discontinuities favors the detachment of limestone pillars and large blocks, which, once isolated, slowly lower or topple from the cliff edges, forming wide debris accumulations (so-called *rdum* by locals). Rdum is the surface finger prints of extensive deep-seated landslides, which dislocate limestone blocks toward the sea.

3 Materials and methods

The landslide susceptibility model was implemented by using the statistical method of the weight of evidence (WoE), which is extensively adopted in geosciences and in landslide susceptibility mapping (Bonham-Carter et al. 1989; Bonham-Carter 1994; Regmi et al.

Fig. 2 Examples of slow-moving landslides (rock spreads and block slides) occurring in the study area

2010 and references therein; Piacentini et al. 2012). This method takes into account the existing relationship between the occurrence of a supporting evidence and the distribution of causal factors that are believed playing an important role in slope instability processes. The weight of the relationship between the presence of deformation and the chosen factor is used to determine the importance of the factor itself. The weighted factors are then combined to create the final susceptibility map.

The implementation of the landslide susceptibility model, through the use of the GIS extension ArcSDM (Sawatzky et al. 2009), needed of the following introductory stages:

1. identification of active mass movements within the area of interest;
2. definition of factors contributing to slope instability and creation of related dataset (including division to appropriate classes).

We used the PSI analysis for the identification of active mass movements (i.e., the supporting evidence) under the assumptions that: (1) The persistent targets on the coast are limestone blocks and (2) the state of activity of the blocks is exclusively attributed to mass movement and no other types of natural or anthropogenic processes.

The objectives of the PSI are as follows: the identification of active block slides, the training of the model and its final validation.

The identification of both structural discontinuities and main coastal landforms that allowed the definition of factors contributing to slope instability (e.g., distance from joints, distance from faults, distance from scarps and distance from coastline) was performed through multi-temporal aerial photograph analysis and published research outcomes (Magri et al. 2008, Devoto et al. 2012). Other complementary morphometric factors (e.g., slope, curvature and Topographic Position Index) were derived from a 2-m resolution DTM of the investigated area.

3.1 Identification of active mass movements by means of PSI analysis

The first step in the implementation of the susceptibility model was the identification of the active landslides within the area of interest. We processed separately 50 ERS and 33 ENVISAT ASAR images acquired on descending orbits. The period of investigation is comprised between 1992 and 2009 with few gaps due to dysfunctional operability of the satellites in 1994, 2001 and 2002. The initial selection of point target candidates was performed based on the low temporal variability of the backscatter radiation (Werner et al. 2003). Beside the expected existence of radar reflectors in urban areas, a good number of natural targets were isolated along the coast. The presence of rock blocks on the clayey slopes and the vertical features of cracks in the Upper Coralline Limestone assisted in the detection of natural point-like reflectors and helped to achieve the minimum number of candidates necessary for a reliable estimate of the atmospheric phase screen (Ferretti et al. 2001). In the test area, we isolated 1320 natural targets (ERS and ENVISAT). We considered as active the PSI with a deformation rate higher than ± 1 mm/year and non-active the rest. This threshold was chosen based on the accuracy achieved from the interferometric analysis and on the characteristics of the investigated phenomena. The 516 active targets (39 % of the total) were afterward divided into subclasses defined by the slope aspect, since radar sensitivity to displacements considerably differs in the north, east and vertical component (Colesanti et al. 2003). That is to say that, assuming that limestone blocks move along the hillside's maximum steepness direction, every active point target on the coast was grouped accordingly. Considering the acquisition geometry of European

Space Agency (ESA) satellites ERS-1/-2 and ENVISAT and the descending orbit, we isolated all the active targets located over slopes with aspect ranging between 270° and 315°, as they were likely to move along the line of sight of the sensor (i.e., the direction along which the radar sensor detects deformations). This procedure led to the selection of 115 persistent scatterers (the 22 % of the active PS inside the aspect range). Based on the assumptions made and on the persistent scatterers selection criteria, we identified 115 active blocks on the test area that were afterward divided into two sets: a training set (60 % of the total) for the statistical analysis and a validation set (40 % of the total) to evaluate the predictive skill of the method.

Figure 3 sums up the results of the PSI analysis in terms of color-coded deformation rates for each persistent scatterer position. As it can be noted, several stretches of the northwestern coast of Malta are affected by deformations that reach a rate of up to 7 mm/year (estimated along the line of sight of the sensor).

3.2 Definitions of factors contributing to slope instability

We identified and tested several factors that could be considered as predisposing to landsliding. Hence, we considered: slope, curvature, the Topographic Position Index (TPI) and distance from coastline, scarps, faults and joints (Fig. 4). The lithology data have not been included in the input spatial dataset since the totality of the 115 persistent scatterers, selected as supporting evidence, accordingly to the above-mentioned assumptions, are limestone blocks. The slope aspect was discarded for its statistical dependency given by the target selection criteria defined above.

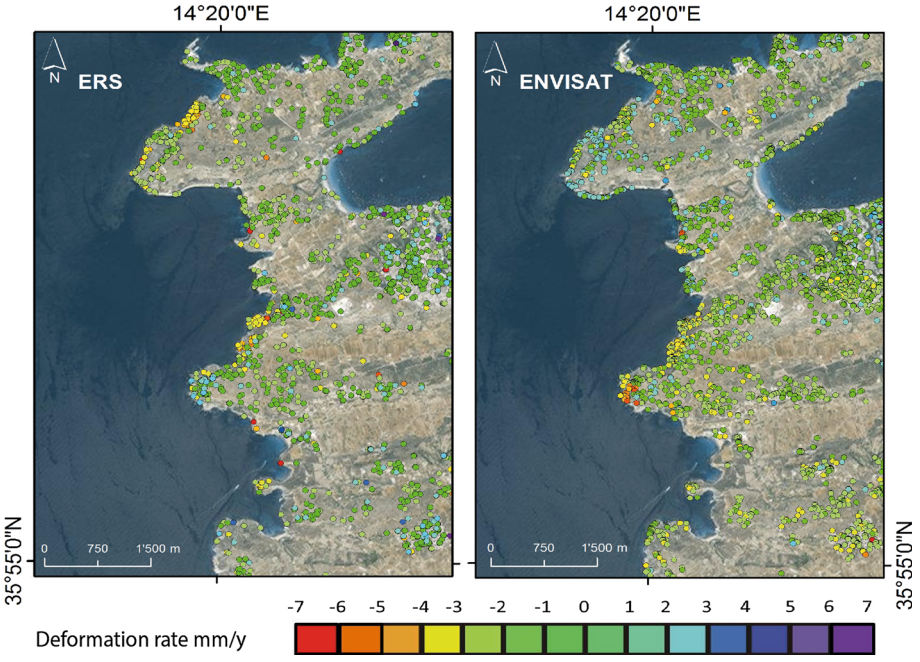

Fig. 3 PSI analysis results of ERS (*left*) and ENVISAT (*right*) dataset superimposed to a Google Earth™ image

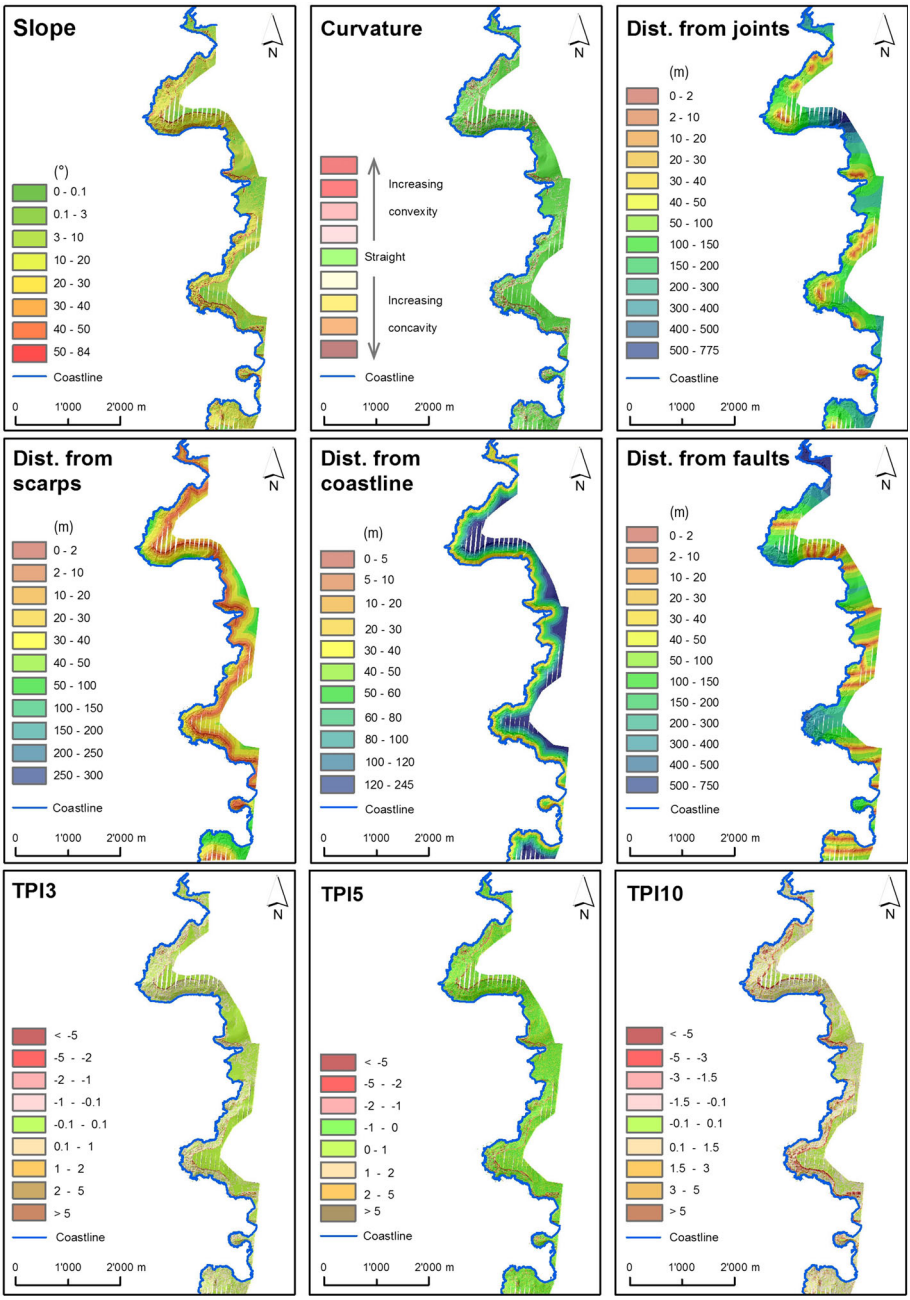

Fig. 4 Maps of the predisposing factors chosen for the statistical analysis

The *slope* is the first derivative of the terrain model and represents the maximum rate of change in value from a cell to its neighbors detecting the steepest path from the cell. The slope values were subdivided into seven classes following an equal area criteria plus an eighth class that includes flat areas.

The *curvature* is the second derivative of the terrain model calculated for each cell position with a computational window of 3 × 3. Using class limits indicated in the literature (e.g., Pereira et al. 2012; Piacentini et al. 2012), the values were divided into three classes: straight slopes, convex and concave.

The *Topographic Position Index* (TPI) is defined as the difference between the elevation of a cell and the average elevation of its neighborhood and is used to describe the relative position of the cells of the DTM with respect to the surrounding area (Jenness et al. 2011). Thus, the TPI is highly scale-dependent (i.e., TPI depends on the radius of the neighborhood considered for its calculation) and enables to quantitatively express the morphology of an area. The TPI is a widely accepted parameter; however, it has begun to be applied in landslide susceptibility modeling (Costanzo et al. 2012; Neuhäuser et al. 2012; Xu et al. 2012; Leopold et al. 2013; Xu et al. 2013) and at different scales only recently (Tagil and Jenness 2008; Vorpahl et al. 2012). In this study, three TPI values taking into account a surrounding area of 3 (TPI^3), 5 (TPI^5) and 10 (TPI^{10}) m, respectively, were calculated. The obtained values were subdivided, considering the natural breaks of each distribution.

The *distances from coastline, scarps, faults and joints* were calculated buffering each lineament over the entire study area with an equidistance of 1 m. Values of these factors were subdivided into different classes, considering the natural breaks of each distribution.

4 Results

The predisposing factors were elaborated as single layers in order to calculate their specific weight and evaluate their different contribution to landslide susceptibility. Figure 5 shows the positive/negative weights and their difference (contrast), resulting from each class of the considered predisposing factors. Only classes with positive contrast exert influence on landslide occurrences.

The validation of every single factor was performed by means of prediction rate curve analysis, considering the cumulative percentage of susceptible areas (starting from the highest susceptibility value) plotted on the *X*-axis and the cumulative percentage of landslide plotted on the *Y*-axis (Fig. 6).

The higher the value of the area under curve (AUC), the better will be the capability of the variable to describe the distribution of landslides. The factors showing the highest values are distance from coastline, distance from joints and distance from scarps (Table 1).

Considering the results of Table 1, 14 different combinations between predisposing factors were calculated and prediction rate curves, built for each combination, compared. The AUC values of the considered combinations are listed in Table 2.

Considering that the best model must simultaneously have good predictive performance and use conditionally independent variables (Pereira et al. 2012) for each combination, the Agterberg and Cheng Conditional Independence test (ACCIT) (Agterberg and Cheng 2002) was also performed. According to this statistic test, models with 1 − (ACCIT/100) below 0.5 have some conditional dependence and below 0.05 should be rejected. Following Pereira et al. (2012), the limit of acceptable conditional independence has been fixed at 0.4 (Fig. 7).

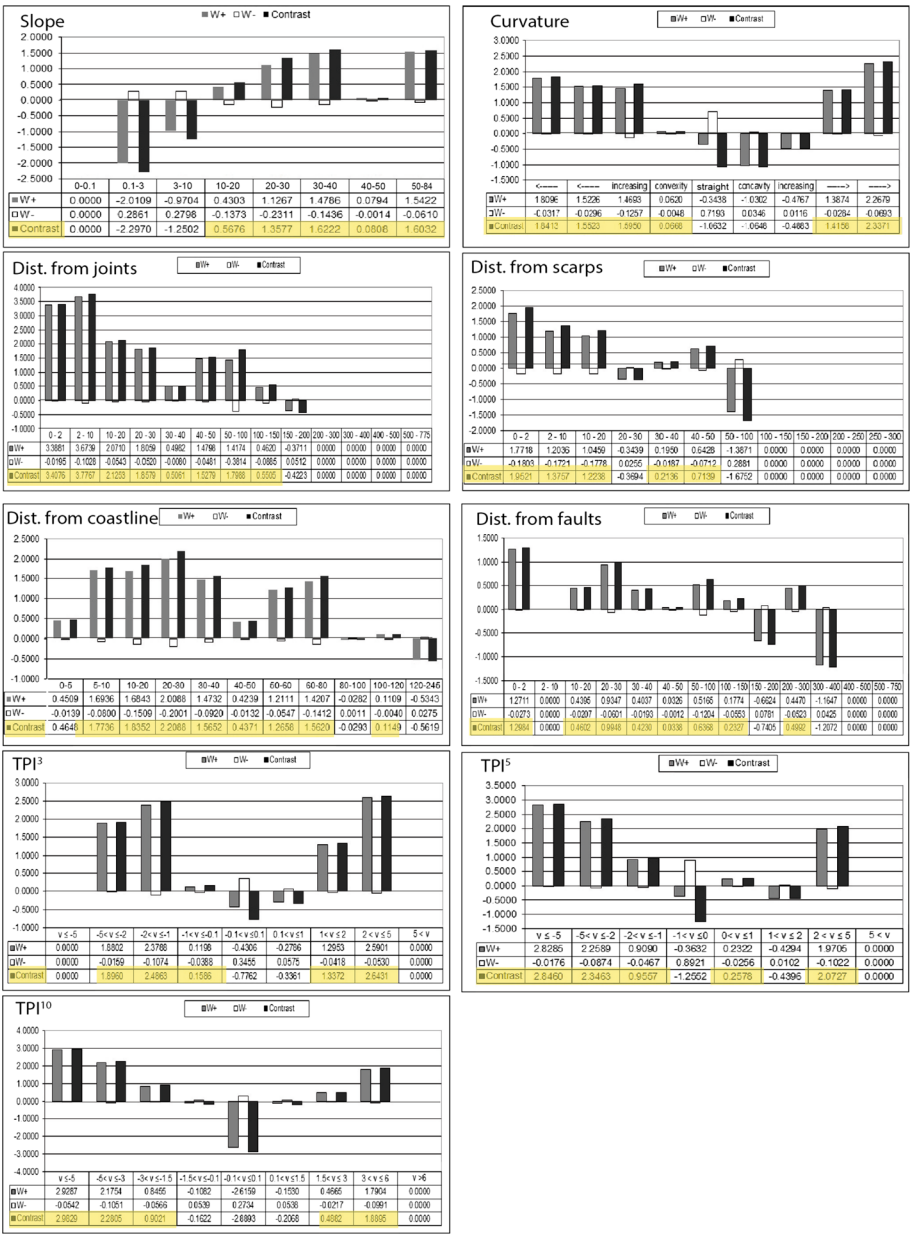

Fig. 5 Graphs showing weights and contrast of each class of predisposing factors. The classes showing positive contrast are highlighted in *yellow*

The best statistical performance (red diamond in Fig. 7) was showed by combination no. 7 that takes into account six predisposing factors (distance from joints, distance from scarps, distance from coastline, TPI^3, TPI^5 and TPI^{10}). Consequently, only the results obtained with this combination are here presented.

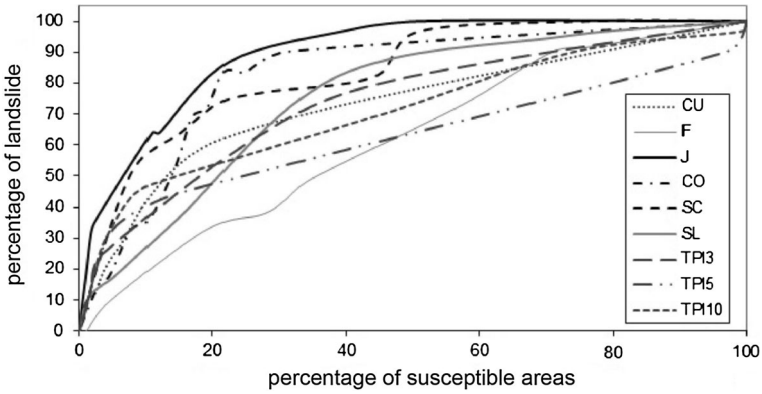

Fig. 6 Prediction rate curves of the predisposing factors: curvature (CU), distance from faults (F), distance from joints (J), distance from coastline (CO), distance from scarps (SC), slope (SL), TPI^3, TPI^5 and TPI^{10}

5 Susceptibility model implementation and validation

In order to produce a landslide susceptibility map based on the results obtained through the statistical computation, the values of post-probability were classified by means of the Jenks natural breaks classification method (Jenks 1967) and four thresholds were selected. These defined the five classes of susceptibility in the map as shown in Fig. 8.

The outcomes of the statistical analysis were validated considering:

(1) independent information not included in the used dataset (validation set);
(2) field surveys;
(3) GNSS measurements.

The first approach allows the estimation of the degree of match between the predicted susceptibility and the independent information not included in the dataset used to construct the model (validation set) (Chung and Fabbri 2003; Guzzetti et al. 2006). The predictive skill has been verified calculating the prediction rate curves, built for the selected combination (distance from joint, distance from scarps, distance from coast, TPI^3, TPI^5 and TPI^{10}). The analysis reports an AUC value of 0.94.

The reliability of the result achieved was then verified through field surveys, and the comparison with a geomorphological map produced at 1:7500 scale by Devoto et al.

Table 1 AUC values of the factors for the validation set

Factor	AUC
Distance from coastline	0.88
Distance from joints	0.87
Distance from scarps	0.83
Slope	0.78
TPI^{10}	0.73
Distance from faults	0.69
TPI^3	0.65
TPI^5	0.64
Curvature	0.63

Table 2 AUC values of the considered combinations between predisposing factors: slope (slope), curvature (curv), distance from coastline (coast), distance from scarps (scarp), distance from faults (fault), distance from joints (joint), TPI^3, TPI^5 and TPI^{10}

Combination number	Predisposing factors	AUC
1	Joint, scarp, slope	0.90
2	Joint, scarp, coast	0.93
3	Joint, scarp, coast, slope	0.93
4	Joint, scarp, coast, TPI^3	0.94
5	Joint, scarp, coast, TPI^5	0.94
6	Joint, scarp, coast, TPI^{10}	0.94
7	**Joint, scarp, coast, TPI^3, TPI^5, TPI^{10}**	**0.95**
8	Joint, scarp, coast, TPI^3, TPI^{10}	0.94
9	Joint, scarp, coast, TPI^3, slope	0.93
10	Joint, scarp, coast, TPI^3, TPI^5, TPI^{10}, slope	0.93
11	Joint, scarp, coast, TPI^3, TPI^5, TPI^{10}, curv	0.94
12	Joint, scarp, coast, TPI^3, TPI^5, TPI^{10}, fault	0.94
13	Joint, scarp, coast, TPI^3, TPI^5	0.93
14	Joint, scarp, coast, TPI^3, TPI^{10}, curv	0.94

Bold is to highlight the combination with the best statistical performance

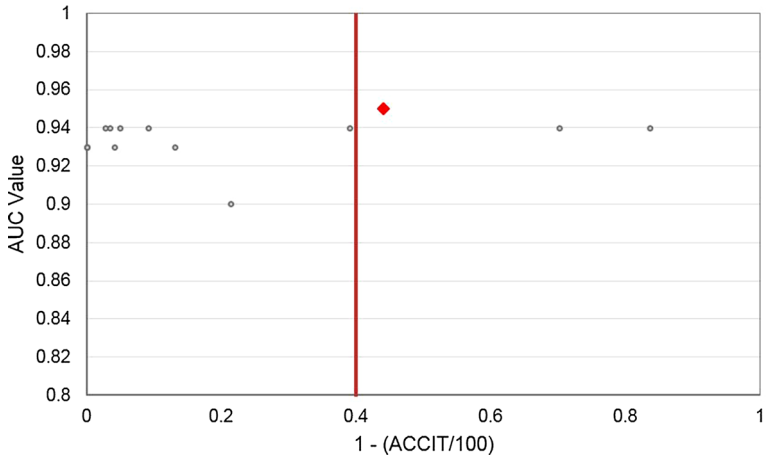

Fig. 7 Scatter plot between AUC values and Agterberg and Cheng Conditional Independence test values of the considered combinations. *Red diamond* shows the selected model. The *red line* marks the limit of acceptable conditional independence

(2012). In this map, 86 landslides affecting the coastal areas have been outlined and classified according to Cruden and Varnes (1996) criteria. The geomorphological observations were compared with the output of the model, with a satisfying fitting between the inventoried block slides and the spatial distribution of high or very high susceptibility class. In particular, the active block slides lying in the northern part of Marfa Ridge, at Il-Prajjet, in the coastal sector between the southern part of Ghadira Bay and Ras Il-Wahx

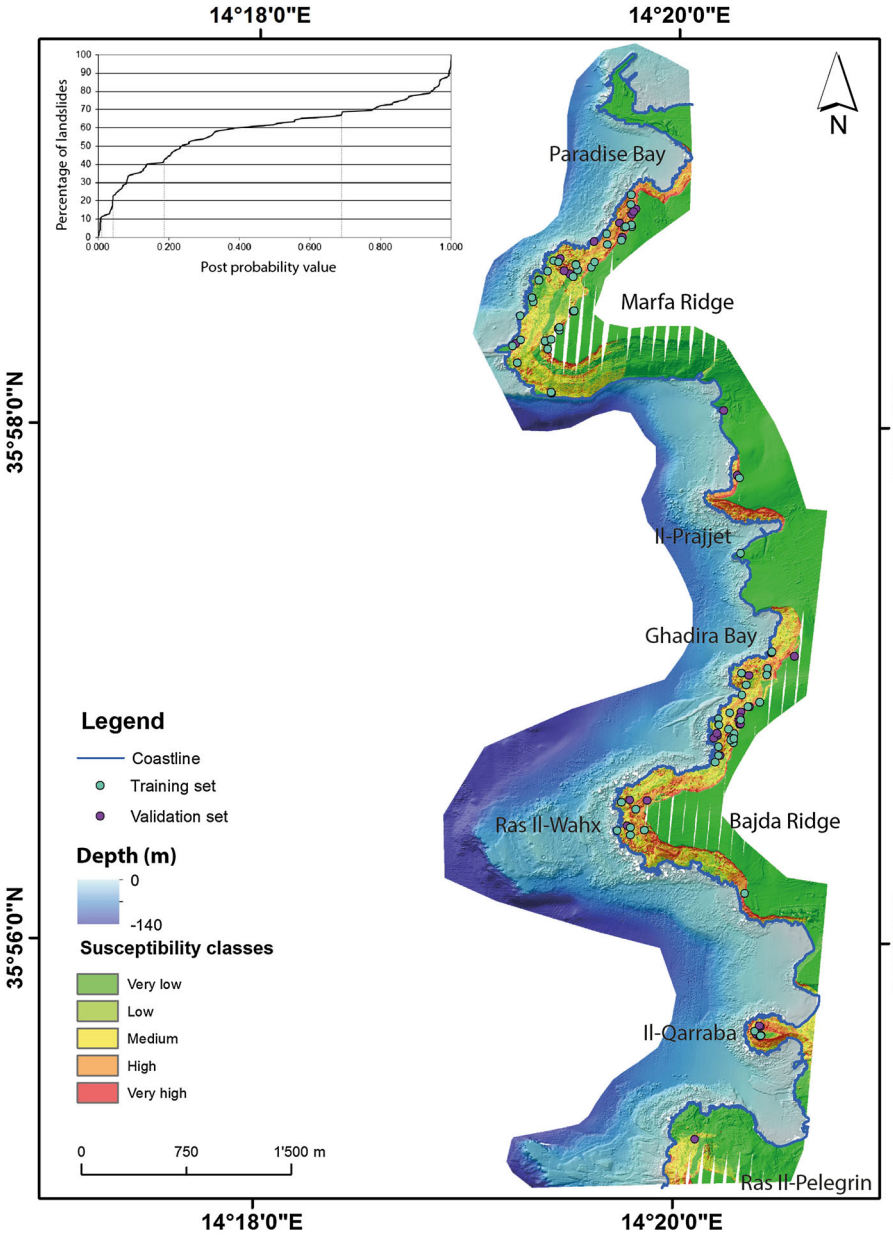

Fig. 8 Landslide susceptibility map of the northwestern coast of Malta

promontory (Fig. 9) and at Il-Qarraba peninsula have been correctly identified by the model. The inventoried landslide was also used as validation set and the degree of match with the model calculated, reporting an AUC value of 0.95.

Finally, the model outputs were quantitatively compared with the surface displacements derived from GNSS campaigns reported in Mantovani et al. (2013). Figure 10 shows the

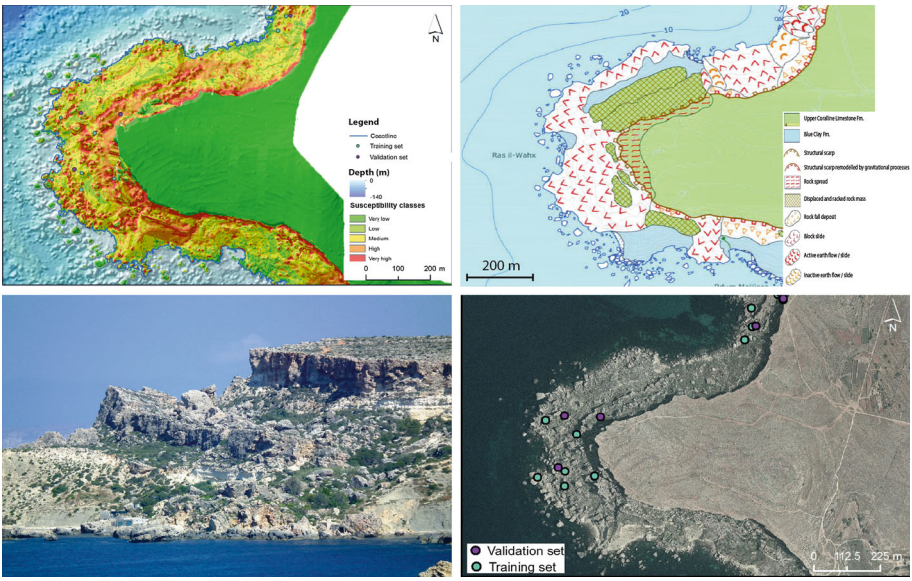

Fig. 9 An example of satisfying fitting between geomorphological observations, inventoried landslides and model results

location of the benchmarks over blocks sliding in one of the most active sectors of the study area (Il-Prajjet).

In the histogram below, the normalized susceptibility at each benchmark location is displayed together with the normalized measured displacements. It can be noticed that decreasing deformation values correspond to lower susceptibility values (anyway included in high and very high classes), proving the reliability of the model. There is a clear quadratic relationship between the variables, meaning that the model overestimates the susceptibility and that this error increases as a second-order polynomial as the real deformations become smaller. In other words, the model is precautionary and works better when the deformation rate of the landslides increases.

6 Discussion

The use of PSI for the production and updating of landslides inventories that could be used as input for susceptibility models has been investigated only recently (see Oliveira et al. 2014), but could represent an effective response to the demand for new cost-effective methods for landslide susceptibility assessment.

The proposed methodology presents the unquestionable advantage that can produce a reliable susceptibility map without using updated and detailed inventory maps that were employed just in the validation step.

The successful results achieved by this approach are strictly correlated with the limited extension of the test site (around 11 km^2), the fairly simple geological and lithological settings and the assumptions on the nature of the radar point targets and on the kinematics of the gravitational processes.

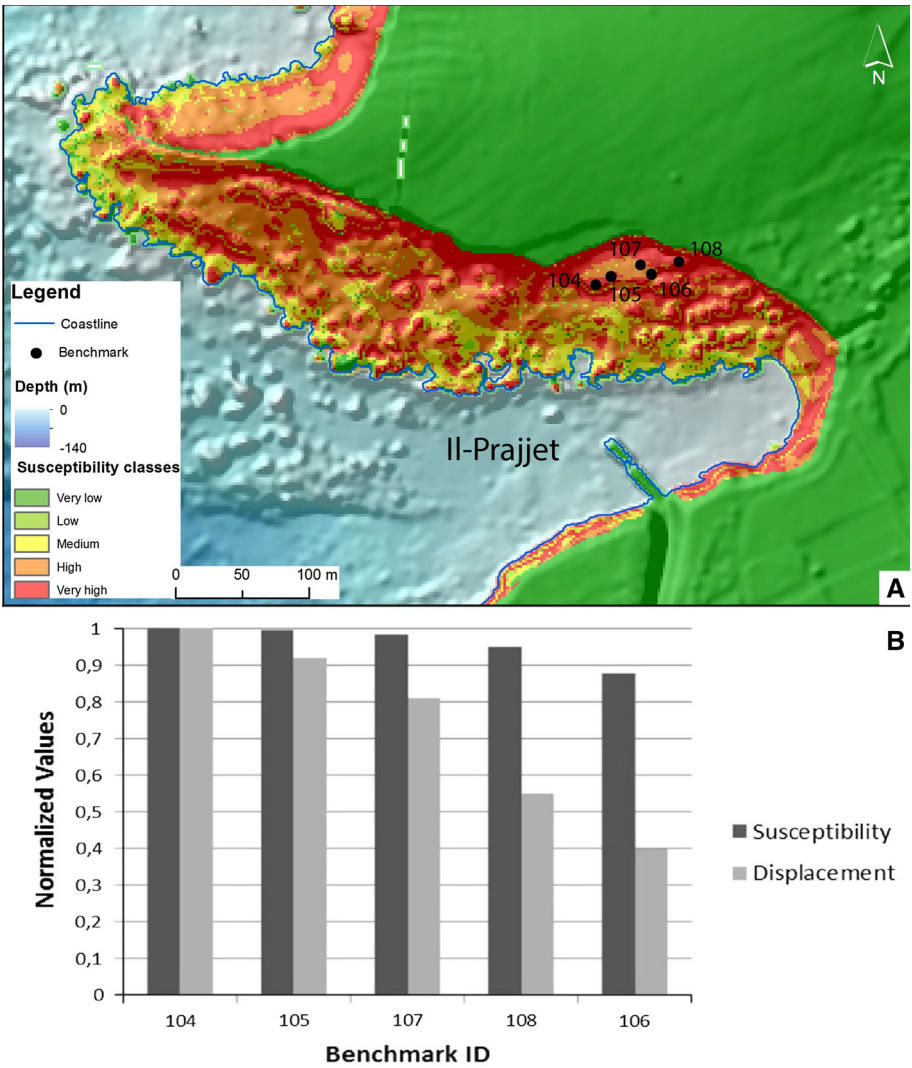

Fig. 10 **a** Location of GNSS benchmarks in one of the most active sectors of the study area monitored by Mantovani et al. (2013) (Il-Prajjet), **b** histogram showing the normalized susceptibility at each benchmark location together with the normalized measured displacement

The procedure we used to implement, test and validate the susceptibility model can be subdivided into four main steps: (1) identification of PSI representative of active mass movements; (2) selection of predisposing factors related to that active mass movements; (3) elaboration of a satisfactory landslide susceptibility model; and (4) independent validation of the results.

Counting the number of cases correctly classified by the model, the points included in the validation set are distributed with respect to the susceptibility classes as follows: 0 % on the very low class, 18.03 % on the low class, 19.67 % on the medium class, 21.31 % on the high class and 40.98 % on the very high class. It is worth noting that approximately

41 % of the total moving PSI, used as validation set, falls into the very high class, which occupies only 2 % of the total area.

In spite of inevitable simplifications and generalizations, the model successfully predicted the active sectors of the coast (e.g., Marfa Ridge, Il-Prajjet, Bajda Ridge and Il-Qarraba) allowing a rapid and cost-efficient delimitation of the sites affected by slow-moving landslides.

7 Conclusions

We implemented a new approach that combines the WoE method and PSI analysis to produce a landslide susceptibility map at a medium scale. We demonstrated the good statistical performance of the model and the reliability of the results that were verified by cross-validation, field surveys and GNSS measurements.

Furthermore, the comparable predictive skills achieved with validation set and inventoried landslides allow extending, with a good degree of confidence, the applicability of the model to areas characterized by similar geological and geomorphological settings even if lacking in inventory map. The susceptibility map obtained is an easy-to-use tool, which can be considered as a starting point for future implementation of hazard analyses. Moreover, it can be applied for land management purposes, assist in hazard mitigation and contribute to decreasing territorial vulnerability. The advantages of using remotely sensed radar datasets in combination with the WoE analysis are multiple. PSI represents the only existing technique that can quantitatively assess the state of activity of landslides at a regional scale with an acceptable cost/efficiency ratio. Compared to the landslide inventories, usually employed as input factors in the WoE, remotely sensed datasets are more accessible, up-to-date and have a unique planetary coverage. Moreover, ESA archives, which were used in this study, span over more than 20 years enabling to perform retrospective researches. The latest space-borne interferometric missions (e.g., COSMO-SkyMed, TerraSAR-X and Sentinel) will increase the spatial and temporal coverage, providing datasets with unprecedented resolution that will certainly favor the implementation of the proposed approach.

Acknowledgments The authors acknowledge European Space Agency for providing ERS and ENVISAT radar images (C1P.7044) and AquaBioTech Group for sharing LiDAR data. The LiDAR survey (HYPERLINK "http://www.airbornehydro.com/hawkeyeii") was carried on HawkEye II of the Airborne Hydrography AB company. SAR processing was performed using Gamma software. The research is part of the project "Coupling terrestrial and marine datasets for coastal hazard assessment and risk reduction in changing environments" funded by the EUR-OPA Major Hazards Agreement of the Council of Europe (responsible M. Soldati). We thank the two anonymous reviewers for their significant comments that helped improving the manuscript.

References

Agterberg FP, Cheng Q (2002) Conditional independence test for weights-of-evidence modelling. Nat Resour Res 11(4):249–255

Alexander D (1988) A review of the physical geography of Malta and its significance for tectonic geomorphology. Quat Sci Rev 7(1):41–53

Bonham-Carter GF (1994) Geographic information systems for geoscientists: modelling with GIS. Pergamon, Ontario

Bonham-Carter GF, Agterberg FP, Wright DF (1989) Weights of evidence modelling: a new approach to mapping mineral potential. In: Agterberg FP, Bonham-Carter GF (eds) Statistical applications in the Earth Sciences: Geological Survey of Canada, 89(9), 171–183

Cardinali M, Reichenbach P, Guzzetti F, Ardizzone F, Antonini G, Galli M et al (2002) A geomorphological approach to the estimation of landslide hazards and risks in Umbria, Central Italy. Nat Hazards Earth Syst Sci 2(1/2):57–72

Cascini L (2008) Applicability of landslide susceptibility and hazard zoning at different scales. Eng Geol 102(3):164–177

Castellanos Abella EA, van Westen CJ (2008) Qualitative landslide susceptibility assessment by multicriteria analysis: a case study from San Antonio del Sur, Guantánamo, Cuba. Geomorphology 94(3):453–466

Chung CJF, Fabbri AG (2003) Validation of spatial prediction models for landslide hazard mapping. Nat Hazards 30(3):451–472

Cigna F, Bianchini S, Casagli N (2013) How to assess landslide activity and intensity with Persistent Scatterer Interferometry (PSI): the PSI-based matrix approach. Landslides 10(3):267–283

Civile D, Lodolo E, Accettella D, Geletti R, Ben-Avraham Z, Deponte M et al (2010) The Pantelleria graben (Sicily Channel, Central Mediterranean): an example of intraplate 'passive'rift. Tectonophysics 490(3):173–183

Colesanti C, Ferretti A, Novali F, Prati C, Rocca F (2003) SAR monitoring of progressive and seasonal ground deformation using the permanent scatterers technique. Geosci Remote Sens Soc IEEE Trans 41(7):1685–1701

Costantini M, Falco S, Malvarosa F, Minati F (2008) A new method for identification and analysis of persistent scatterers in series of SAR images. In: International Geoscience and Remote Sensing Symposium, 2008. IGARSS 2008. IEEE International (vol 2, pp. II–449). IEEE

Costanzo D, Rotigliano E, Irigaray C, Jiménez-Perálvarez JD, Chacón J (2012) Factors selection in landslide susceptibility modelling on large scale following the gis matrix method: application to the river Beiro basin (Spain). Nat Hazards Earth Syst Sci 12:327–340

Cruden DM, Varnes DJ (1996) Landslides investigation and mitigation, transportation research board. In: Turner AK, Schuster RL (eds) Landslide types and process, National Research Council, National Academy Press, Special Report, 247, 36–75

Cyffka B, Bock M (2008) Degradation of field terraces in the Maltese Islands—reasons, processes, and effects. Geogr Fis Din Quat 31(2):119–128

Dart CJ, Bosence DWJ, McClay KR (1993) Stratigraphy and structure of the Maltese graben system. J Geol Soc 150(6):1153–1166

Devoto S, Biolchi S, Bruschi VM, Furlani S, Mantovani M, Piacentini D et al (2012) Geomorphological map of the NW Coast of the Island of Malta (Mediterranean Sea). J Maps 8(1):33–40

Devoto S, Biolchi S, Bruschi VM, Díez AG, Mantovani M, Pasuto A et al (2013) Landslides along the northwest coast of the Island of Malta. In: Margottini C et al (eds) Landslide science and practice, vol 1. Springer, Berlin Heidelberg, pp 57–63

Dykes AP (2002) Mass movements and conservation management in Malta. J Environ Manag 66(1):77–89

Ferretti A, Prati C, Rocca F (2001) Permanent scatterers in SAR interferometry. Geosci Remote Sens IEEE Trans 39(1):8–20

Galve JP, Cevasco A, Brandolini P, Soldati M (2015) Assessment of shallow landslide risk mitigation measures based on land use planning through probabilistic modelling. Landslides 12(1):101–114

Guzzetti F, Carrara A, Cardinali M, Reichenbach P (1999) Landslide hazard evaluation: a review of current techniques and their application in a multi-scale study, Central Italy. Geomorphology 31(1):181–216

Guzzetti F, Reichenbach P, Ardizzone F, Cardinali M, Galli M (2006) Estimating the quality of landslide susceptibility models. Geomorphology 81(1):166–184

Illies JH (1981) Graben formation—the Maltese Islands—a case history. Tectonophysics 73(1):151–168

Jenks GF (1967) The data model concept in statistical mapping. Int Yearb Cartogr 7(1):186–190

Jenness J, Brost B, Beier P (2011) Land facet corridor designer: extension for ArcGIS. Jenness Enterprises, Flagstaff

Jongsma D, van Hinte JE, Woodside JM (1985) Geologic structure and neotectonics of the North African continental margin south of Sicily. Mar Pet Geol 2(2):156–179

Lan HX, Zhou CH, Wang LJ, Zhang HY, Li RH (2004) Landslide hazard spatial analysis and prediction using GIS in the Xiaojiang watershed, Yunnan, China. Eng Geol 76(1):109–128

Leopold P, Heiss G, Petschko H, Bell R, Glade T (2013) Susceptibility maps for landslides using different modelling approaches. In: Margottini C et al (eds) Landslide science and practice, vol 1. Springer, Berlin Heidelberg, pp 353–356

Lu P, Catani F, Tofani V, Casagli N (2014) Quantitative hazard and risk assessment for slow-moving landslides from Persistent Scatterer Interferometry. Landslides 11(4):685–696
Magri O, Mantovani M, Pasuto A, Soldati M (2008) Geomorphological investigation and monitoring of lateral spreading along the north-west coast of Malta. Geogr Fis Din Quat 31(2):171–180
Mantovani M, Devoto S, Forte E, Mocnik A, Pasuto A, Piacentini D et al (2013) A multidisciplinary approach for rock spreading and block sliding investigation in the north-western coast of Malta. Landslides 10(5):611–622
Martino S, Mazzanti P (2014) Integrating geomechanical surveys and remote sensing for sea cliff slope stability analysis: the Mt. Pucci case study (Italy). Nat Hazards Earth Syst Sci 14:831–848
Neuhäuser B, Damm B, Terhorst B (2012) GIS-based assessment of landslide susceptibility on the base of the weights-of-evidence model. Landslides 9(4):511–528
Oliveira SC, Zêzere J, Catalão J, Nico G (2014) The contribution of PSInSAR interferometry to landslide hazard in weak rock-dominated areas. Landslides. doi:10.1007/s10346-014-0522-9
Pasuto A, Soldati M (2013) Lateral spreading. In: Shroder JF, Marston RA, Stoffel M (eds) Treatise on geomorphology, vol 7. Mountain and Hillslope geomorphologyAcademic Press, San Diego, pp 239–248
Pedley M, Clarke MH (2002) Limestone Isles in a Crystal Sea: the geology of the Maltese Islands. Publishers Enterprises Group, San Gwann
Pereira S, Zêzere JL, Bateira C (2012) Technical note: assessing predictive capacity and conditional independence of landslide predisposing factors for shallow landslide susceptibility models. Nat Hazards Earth Syst Sci 12:979–988
Piacentini D, Troiani F, Soldati M, Notarnicola C, Savelli D, Schneiderbauer S et al (2012) Statistical analysis for assessing shallow-landslide susceptibility in South Tyrol (south-eastern Alps, Italy). Geomorphology 151:196–206
Raucoules D, Colesanti C, Carnec C (2007) Use of SAR interferometry for detecting and assessing ground subsidence. Comptes Rendus Geosci 339(5):289–302
Regmi NR, Giardino JR, Vitek JD (2010) Modeling susceptibility to landslides using the weight of evidence approach: Western Colorado, USA. Geomorphology 115(1):172–187
Righini G, Pancioli V, Casagli N (2012) Updating landslide inventory maps using Persistent Scatterer Interferometry (PSI). Int J Remote Sens 33(7):2068–2096
Sawatzky DL, Raines GL, Bonham-Carter GF, Looney CG (2009) Spatial Data Modeller (SDM): ArcMAP 9.3 geoprocessing tools for spatial data modelling using weights of evidence, logistic regression, fuzzy logic and neural networks and neural networks. http://arcscripts.esri.com/details.asp?dbid=15341. Accessed 24 June 2014
Soldati M, Maquaire O, Zezere JL, Piacentini D, Lissak C (2011) Coastline at risk: methods for multi-hazard assessment. J Coast Res Spec Issue 61:335–339
Tagil S, Jenness J (2008) GIS-based automated landform classification and topographic, landcover and geological attributes of landforms around the Yazoren Polje, Turkey. J Appl Sci 8(6):910–921
van Westen CJ, Castellanos E, Kuriakose SL (2008) Spatial data for landslide susceptibility, hazard, and vulnerability assessment: an overview. Eng Geol 102(3):112–131
Vorpahl P, Elsenbeer H, Märker M, Schröder B (2012) How can statistical models help to determine driving factors of landslides? Ecol Model 239:27–39
Werner C, Wegmuller U, Strozzi T, Wiesmann A (2003) Interferometric point target analysis for deformation mapping. In: International Geoscience and Remote Sensing Symposium, 2003. IGARSS'03. Proceedings. 2003 IEEE International (vol. 7, pp. 4362–4364). IEEE
Xu C, Xu X, Lee YH, Tan X, Yu G, Dai F (2012) The 2010 Yushu earthquake triggered landslide hazard mapping using GIS and weight of evidence modelling. Environ Earth Sci 66(6):1603–1616
Xu C, Xu X, Yao Q, Wang Y (2013) GIS-based bivariate statistical modelling for earthquake-triggered landslides susceptibility mapping related to the 2008 Wenchuan earthquake, China. Q J Eng Geol Hydrogeol 46:221–236